Inorganic Chemistry

Article

pubs.acs.org/IC

Triphos Iridium(III) Halide Complex Photochemistry: Triphos Arm Dissociation

Andreas Ross and Paul R. Sharp*

Department of Chemistry, University of Missouri-Columbia, 125 Chemistry Building, Columbia, Missouri 65211-7600, United States

Supporting Information

ABSTRACT: Photolysis of Ir(triphos)X_3 (triphos = 1,1,1-tris(diphenylphosphinomethyl)ethane; X = Cl, Br) yields an insoluble product believed to be oligomeric $[Ir(triphos)X_3]_n$ with bridging triphos and halide ligands. Refluxing pyridine (py) dissolves the insoluble photoproducts ultimately yielding the dangling triphos complexes *mer*-Ir(κ^2-triphos)(py)X_3. Oxidation of the P center of the dangling arm of Ir(κ^2-triphos)(py)Cl_3 yields *mer*-Ir(κ^2-P,P-triphosO)(py)Cl_3 (triphosO = $MeC(CH_2P(O)Ph_2)(CH_2PPh_2)_2$), which was characterized by single-crystal X-ray diffraction. *mer*-Ir(κ^2-triphos)(py)Cl_3 is also formed when Ir(triphos)Cl_3 is photolyzed in the presence of py (ϕ = 26%). Both *mer*-Ir(κ^2-triphos)(py)Cl_3 and *mer*-Ir(κ^2-P,P-triphosO)(py)Cl_3 photoisomerize in pyridine to their thermally unstable *fac*-isomers. Density functional theory (DFT) and time-dependent DFT (TDDFT) calculations suggest triphos ligand arm dissociation occurs along a triplet pathway from an initial Franck−Condon ligand-field excited state that relaxes to a Jahn−Teller axially distorted octahedral triplet with a long Ir−P bond. Subsequent triphos arm dissociation yields a distorted trigonal-bipyramidal triplet that undergoes intersystem crossing to a square pyramidal singlet.

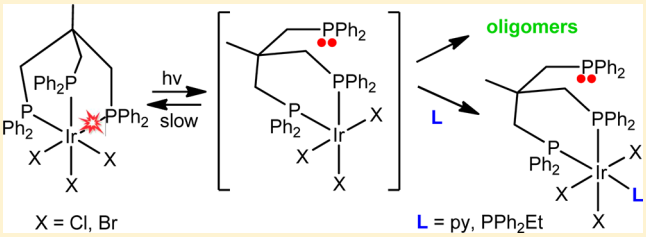

INTRODUCTION

We recently reported efficient net photochemical bromine elimination from Pt(IV) polyhalide complexes (eq 1),[1] an important process in potential solar energy conversion and storage.[2] Wishing to expand this chemistry to other transition metal d^6-systems we became interested in the photochemistry of octahedral Ir(III) polyhalide complexes.

$$trans\text{-}PtL_2(R)Br_3 \xrightarrow{light} trans\text{-}PtL_2(R)Br + Br_2 \quad (Br_2 \text{ trapped by alkenes}) \qquad (1)$$

Iridium(III) complexes are involved in a number of photochemical processes. Recently, they have been studied especially as phosphorescent dyes in the field of organometallic light emitting diodes (OLEDs) because of their excellent color tuning.[3,4] Ford and co-workers[5,6] observed photoaquation (eq 2) and photoinduced ligand exchange of iridium(III) complexes. Photoisomerization (eq 3)[7−9] and photochemical reductive elimination of molecular oxygen, molecular hydrogen, and hydrogen chloride have also been reported (eq 4, XY = O_2, H_2, HCl),[10] the latter suggesting that Ir(III) complexes may also undergo halogen photoelimination.

$$[IrL_6]^{3+} + H_2O \overset{light}{\rightleftharpoons} [IrL_5(H_2O)]^{3+} + L \qquad (2)$$

$$mer\text{-}IrCl_3L_3 \xrightarrow{light} fac\text{-}IrC_3L_3 \qquad (3)$$

$$L_3IrCl(X)(Y) \xrightarrow{light} L_3IrCl + XY \qquad (4)$$

To suppress isomerization (eq 3), we chose to investigate octahedral Ir(III) complexes with tridentate ligands that would disfavor ligand exchange and isomerization and perhaps show other photochemical processes such as halogen photoelimination (eq 4, X = Y = a halogen). Herein we report our photochemical investigation of iridium(III) trihalide complexes with the tripodal ligand triphos (1,1,1-tris(diphenylphosphinomethyl)ethane), which locks in a *fac* configuration of the halide ligands. (For other examples of Ir tripodal phosphine systems see references 11−14.) While the triphos complexes show rich dissociative photochemistry, halogen elimination is not observed.

RESULTS

Complex Synthesis and Characterization. Known trichloro complex Ir(triphos)Cl_3 (**1**) was prepared by a literature procedure (eq 5)[15] and its molecular structure determined by single-crystal X-ray analysis (Figure 1). (The synthesis and structure of analogous *fac*-Ir$(PMe_3)_3Cl_3$ was recently reported.[16]) Although not mentioned in the original synthesis of **1**, in our hands known[17] hydride complex Ir(triphos)Cl_2H (**2**) is always present as a byproduct. This hydride complex is probably formed from the reaction of **1** with the 2-methoxyethanol solvent, and prolonged heating of **1** in 2-methoxyethanol gives good yields of **2** (eq 6). This probably also explains the need for NaCl in the synthesis of **1**, excess Cl^- would inhibit formation of alkoxo complexes with the 2-methoxyethanol and subsequent hydride formation. Leaving out the NaCl in the synthesis of **1** yields a black precipitate of

Received: July 16, 2013
Published: October 18, 2013

   dx.doi.org/10.1021/ic401835d | *Inorg. Chem.* 2013, 52, 12645−12654

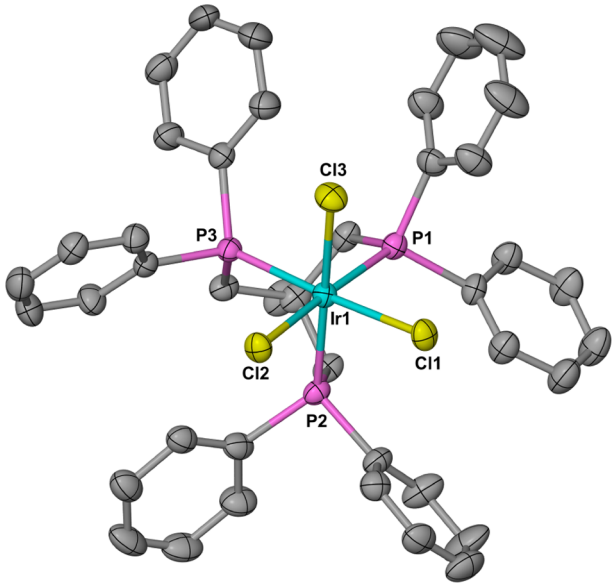

Figure 1. Solid-state structure of Ir(triphos)Cl_3 **1** (50% thermal ellipsoids, hydrogen atoms omitted and carbon atoms unlabeled).

unknown composition, probably from reduction of starting $IrCl_3(H_2O)_x$ prior to formation of **1**.

$$IrCl_3(H_2O)_x \xrightarrow[\text{reflux, 16 h, 2-methoxyethanol}]{\text{triphos, NaCl}} \underset{\mathbf{1}}{\text{Ir(triphos)Cl}_3} \quad (5)$$

$$\mathbf{1} \xrightarrow[\text{2-methoxyethanol}]{\text{reflux, 24 h}} \underset{\mathbf{2}}{\text{Ir(triphos)Cl}_2\text{H}} \quad (6)$$

The bromo analogue of **1**, Ir(triphos)Br_3 (**3**), is readily obtained from **1** in quantitative yield by heating (40 °C) **1** with KBr in freshly distilled acetone (eq 7). The same reaction in "bulk" acetone yields the bromohydride Ir(triphos)Br_2H (**4**) (eq 8). Again, hydride formation most likely involves alkoxo complexes, in this case from alcohol impurities in the acetone.

$$\mathbf{1} \xrightarrow[\text{40 °C, 24 h acetone}]{\text{KBr}} \underset{\mathbf{3}}{\text{Ir(triphos)Br}_3} \quad (7)$$

$$\mathbf{1} \xrightarrow[\text{40 °C, 48 h, "bulk" acetone}]{\text{KBr}} \underset{\mathbf{4}}{\text{Ir(triphos)Br}_2\text{H}} \quad (8)$$

Characterization of new Ir(triphos)Br_3 (**3**) and Ir(triphos)-Br_2H (**4**) is through ^{31}P and ^{1}H NMR spectroscopy and single crystal X-ray diffraction (**4**, see Supporting Information). Complex **3** has a single resonance at δ −37 in its $^{31}P\{^1H\}$ NMR spectrum (CH_2Cl_2). The $^{31}P\{^1H\}$ NMR spectrum (CD_2Cl_2) of **4** is very similar to that of **2** and shows two resonances in a 2:1 ratio, a doublet (J_{PP} = 11.2 Hz) at δ −13.1 and a triplet at δ −50.8. The ^{1}H NMR spectrum (CD_2Cl_2) shows a hydride resonance at δ −8.78 as a doublet of triplets (J_{HP} = 181 Hz, J_{HP} = 8.8 Hz).

UV−vis spectra for the trihalo complexes **1** and **3** are presented in Figure 2. As expected for the white to pale yellow complexes, strong absorption is only observed in the uv region with weak tail-offs into the visible.

Photochemistry. Photolysis (313 nm) of **1** or **3** in the presence or absence of 1-hexene causes the yellow solution to bleach and pale yellow precipitates (**5** and **6**, respectively) to form (eq 9). Precipitates **5** and **6** are formulated as oligomeric forms of **1** and **3** (see below) and can be converted back to **1** and **3** simply by refluxing in 2-methoxyethanol for 16 h (eq 9). (Refluxing for longer periods (48 h) yields hydride complexes Ir(triphos)(H)Cl_2 (**2**) and Ir(triphos)Br_2H (**4**) (see eq 6 and 8).)

$$\underset{\mathbf{1}(X=Cl)\ \mathbf{3}(X=Br)}{\text{Ir(triphos)X}_3} \underset{\text{reflux, 16 h}}{\overset{\text{313 nm, CH}_2\text{Cl}_2}{\rightleftharpoons}} \underset{\text{2-methoxyethanol}}{[\underset{\mathbf{5}(X=Cl)\ \mathbf{6}(X=Br)}{\text{Ir(triphos)X}_3}]_n} \quad (9)$$

Elemental analysis, solid state IR, and ^{31}P NMR spectroscopy were used to more completely characterize photoproduct **5**. Elemental analysis of **5** is essentially identical to **1** except with incorporation of small and variable amounts of solvent (CH_2Cl_2) that could not be removed in vacuo but were detected (^{1}H NMR) by dissolving (see below) the solid in pyridine-d_5. The KBr pellet IR spectrum of **5** and **1** are also essentially identical (Supporting Information) suggesting that the triphos ligand is intact in the photoproduct. The far IR (mineral oil mull) spectra, however, differ (Supporting Information). That of **1** shows two Ir−Cl stretching bands at 303 and 278 cm^{-1}, characteristic of *facial* terminal chloro

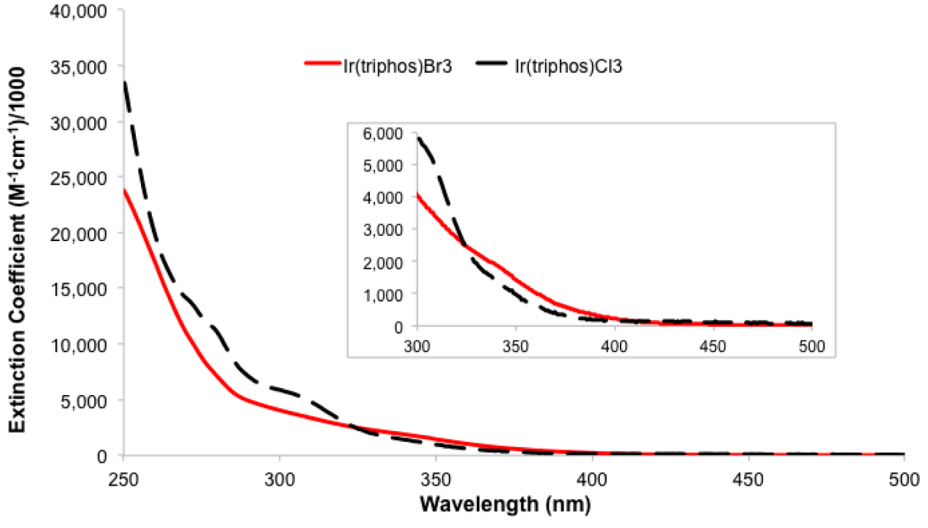

Figure 2. UV−vis spectra for Ir(triphos)Cl_3 **1** (black dashed line) and Ir(triphos)Br_3 **3** (red solid line) in dichloromethane.

dx.doi.org/10.1021/ic401835d | *Inorg. Chem.* 2013, 52, 12645−12654

ligands *trans* to phosphine ligands.[18−21] The far IR spectrum of **5** also shows bands at 303 and 278 cm^{-1} but strong, broad bands also appear at higher energy (324 and 317 cm^{-1}) and lower energy (264 cm^{-1}). The higher energy bands indicate the presence of chloro ligands *trans* to weaker donors than a phosphine ligand (e.g., terminal or bridging chloro ligands) and the lower energy band is consistent with bridging chloro ligands. The solid-state ^{31}P NMR spectrum of **5** shows multiple broad peaks from δ 9 to −90 suggesting multiple environments for the P centers in solid **5**. The largest peak occurs at δ −32 in a region similar to that for **1** and **2** in solution.

Precipitates **5** and **6** are generally insoluble but dissolve in pyridine to give initial ^{31}P NMR spectra with a plethora of peaks (Supporting Information) indicating a complex product or mixtures. Heating a pyridine solution of **5** at 120 °C (sealed tube) under argon overnight gives a single product identified as the dangling triphos complex *mer*-Ir(κ^2-triphos)(py)Cl_3 (**7**) (eq 10). Complex **1** is stable under these conditions indicating that

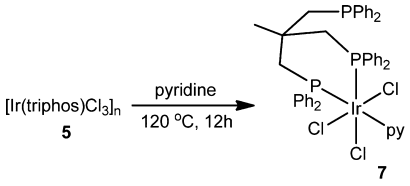

(10)

1 is not a product of dissolving **5** in pyridine. The ^{31}P NMR spectrum of **7** in $CDCl_3$ or CH_3NO_2 shows the dangling phosphine group as a broad peak at δ −26.6, near the signal for free triphos (δ −25.3). The coordinated phosphine group signals are found at δ −29.1 and −41.0 and are coupled to each other ($^2J_{PP}$ = 24 Hz). Surprisingly, the signal at δ −29.1 shows weak coupling to the dangling phosphine group ($^4J_{PP}$ = 2 Hz). In pyridine or benzene, the coupling increases to 4 Hz, and the dangling phosphine group signal sharpens into a doublet, also with 4 Hz coupling. ^1H NMR signals for one of the three diastereotopic triphos methylene groups are broad in $CDCl_3$ and probably belong to the dangling phosphine group. The changes in P−P coupling and broadness of the dangling phosphine group signals is likely due to hindered rotation about the C−C and P−C bonds of the dangling phosphine group with two or more rotational conformations. The lowest energy conformation must be such that four-bond P−P coupling is possible, but the coupling is lost in other conformations. (Conformation-dependent, long-range P−P coupling has been previously observed.[22]) Consistent with this, heating a CH_3NO_2 NMR sample to 80 °C causes collapse of the dangling phosphine group signal and complete loss of coupling to the Ir-bonded phosphine group. The favoring of the one conformation by pyridine and benzene is likely due to $\pi-\pi$ interactions between the pyridine and the triphos phenyl rings.

Complex **7** is oxygen sensitive and tends to undergo slow oxidation of the dangling phosphine group. (Dangling triphos ligand oxidation has been reported.[23,24]) Rapid oxidation of **7** with hydrogen peroxide gives *mer*-Ir(κ^2-*P,P*-triphosO)(py)Cl_3 (**8**, triphosO = $MeC(CH_2P(O)Ph_2)(CH_2PPh_2)_2$) (eq 11), which readily yielded crystals suitable for X-ray diffraction analysis (Figure 3). NMR data for **8** are similar to **7** except that the dangling phosphine group signal is absent and converted to a dangling phosphine oxide group signal at δ 27.1, and all signals are sharp. Presumably, conversion of the dangling phosphine group to a phosphine oxide group results in a conformation that does not allow four-bond P−P coupling,

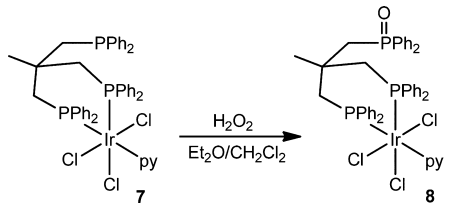

(11)

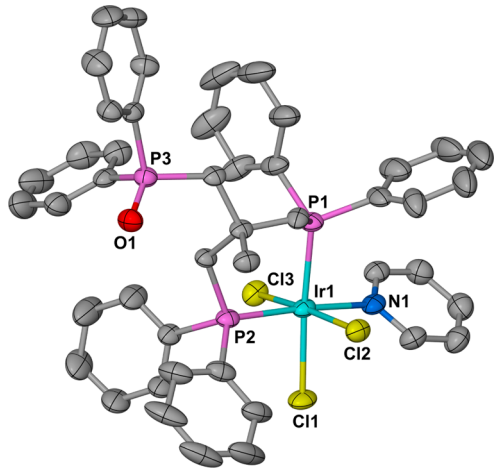

Figure 3. Solid-state structure of *mer*-Ir(κ^2-P,P-triphosO)(py)Cl_3 **8** (50% thermal ellipsoids, hydrogen atoms omitted, and carbon atoms unlabeled).

although the change in oxidation state of the phosphorus center could also affect coupling. As with **8**, heating the NMR sample causes collapse of the dangling phosphine oxide group signal indicating the presence of multiple conformations.

Complex **1** also dissolves in pyridine but without reaction. However, photolysis results in efficient conversion, first to **7**, but with continued irradiation a new product (**9**) grows in (Scheme 1). Continued irradiation, after **1** is completely

Scheme 1

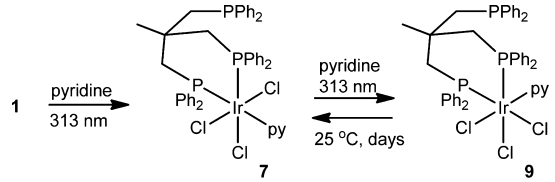

consumed, converts **7** into **9**. The ^{31}P NMR spectrum of **9** in $CDCl_3$ shows two peaks in a 1:2 ratio with the smaller peak (δ −27.8) in the same region as the dangling phosphine group of **7**. The larger peak (δ −38.7) is in a similar region to that of one of the bonded phosphine groups of **7** and **8**. (These peaks are assigned to a P atom *trans* to a Cl ligand.) Complex **9** is assigned as the *facial* isomer of *meridional* **7**, that is *fac*-Ir(κ^2-triphos)(py)Cl_3 with the py *trans* to a Cl instead of a P group as in **7** and **8**. Similar to **7**, **9** shows evidence of a conformation of the dangling phosphine group that gives rise to four-bond P−P coupling. In pyridine and benzene, coupling between the dangling phosphine group and the coordinated phosphine groups is evident, and the coordinated phosphine group signal at δ −38.7 becomes a doublet and the smaller signal for the dangling phosphine group becomes a triplet (J_{PP} = 4 Hz). Complex **9** slowly (days) reverts to **7** in solution and was always isolated with small amounts of **7**. Complex **7** is also

dx.doi.org/10.1021/ic401835d | *Inorg. Chem.* 2013, 52, 12645−12654

obtained from the 380 nm photolysis of **1** in dichloromethane with added pyridine. These conditions were used to avoid absorption by pyridine and to obtain the quantum yield (0.26 ± 0.04) for the photolysis.

When a CH_2Cl_2 solution of **1** is photolyzed with PPh_2Et a new soluble product is formed (eq 12). Although not isolated,

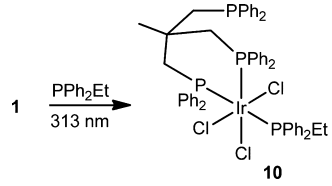

(12)

the ^{31}P NMR spectrum is fully consistent with the formation of the PPh_2Et analogue of **7**, *mer*-Ir(κ^2-triphos)(PPh_2Et)Cl_3 (**10**). The dangling phosphine signal is a singlet at δ −28, the PPh_2Et signal is a double doublet at δ −16.8 and shows very strong *trans* coupling (442 Hz) to one of the coordinated triphos P atoms and much weaker *cis* coupling (16 Hz) to the other coordinated triphos P atom. The coordinated triphos P atom signals are also double doublets (*trans* to PPh_2Et: δ −35.6, *trans* to Cl: δ −48.8) and with *cis* coupling to each other of 19 Hz.

Prolonged (24 h) photolysis of a pyridine solution of **1** under air results in phosphine oxidation and formation of the *facial* isomer of **8**, *fac*-Ir(κ^2-P,P-triphosO)(py)Cl_3 (**11**, Scheme 2).

Scheme 2

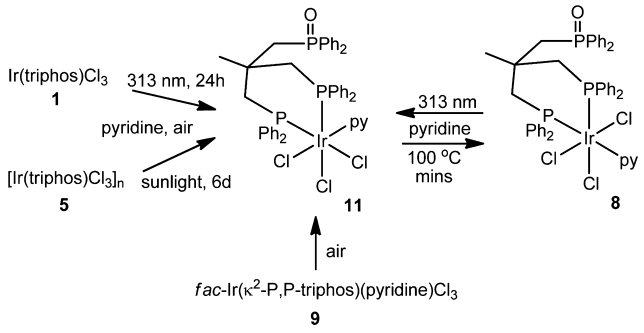

Complex **11** is also formed in three other ways: when photoproduct **5** is dissolved in pyridine and then the solution is exposed to sunlight for 6 days in air, by photolysis of the *meridional* isomer **8**, or by air oxidation of **9**. The ^{31}P NMR spectrum of **11** shows two peaks in a 1:2 ratio. The smaller peak is found at δ 25.7, in the same region as the dangling PO group of **8**. The larger peak is observed at δ −39.3, in the same region as that for the bonded P groups of **9**. *Facial* **11** slowly (days) converts to *meridional* **8** at room temperature in dichloromethane solution, or rapidly (min) at 100 °C in pyridine, indicating that, as with **7** and **9**, the *meridional* isomer is the thermally more stable isomer.

DFT Calculations. To better understand the photoactivity of the iridium(III) complexes a density functional theory (DFT) study (M06/LANL2DZ (X = Cl) or B3LYP/LANL2DZ (X = Br)) was undertaken. The mean metrical parameters (Table 1) for the DFT optimized geometry $\mathbf{1}^{S6}$ ($\mathbf{3}^{S6}$ for the bromo analogue) and the X-ray structure of **1** are in good agreement with the Ir-ligand distances being slightly longer (4% or less) in the DFT structure. (The greater variation in the equivalent bond distances for the DFT structure (see esd's) may be at least partly due to a slightly different phenyl ring arrangement resulting in different intramolecular contacts.) Using the X-ray crystal structure coordinates of **1** as starting coordinates for triplet optimization yielded 5-coordinate $\mathbf{1}^{T5}$ (Figure 4). Again starting from the X-ray crystal structure coordinates of **1** but changing the chloro ligands to bromo ligands (i.e., **3**) gave 6-coordinate $\mathbf{3}^{T6}$. Exchanging the bromo ligands of $\mathbf{3}^{T6}$ for chloro ligands followed by optimization gave 6-coordinate triplet structure $\mathbf{1}^{T6}$ (Figure 4) and exchanging the chloro ligands of $\mathbf{1}^{T5}$ for bromo ligands gave 5-coordinate triplet $\mathbf{3}^{T5}$. Metrical parameters for the triplet structures are listed in Table 2. The 5-coordinate triplet structures ($\mathbf{1}^{T5}$ and $\mathbf{3}^{T5}$) show a 5-coordinate, distorted trigonal bipyramidal Ir center geometry with one arm of the triphos ligand completely dissociated. The coordinated portion of the triphos ligand occupies an axial (P1) and an equatorial (P2) position. The 6-coordinate triplet structures ($\mathbf{1}^{T6}$ and $\mathbf{3}^{T6}$) show an axially distorted octahedral geometry with elongation of one set of *trans* Ir−P and Ir−X bonds (Ir−P3 and Ir−X3). The 5-coordinate chloro triplet ($\mathbf{1}^{T5}$) is isoenergetic with its 6-coordinate analogue ($\mathbf{1}^{T6}$) while the bromo 5-coordinate triplet ($\mathbf{3}^{T5}$) is 12 kcal lower than the 6-coordinate triplet ($\mathbf{3}^{T6}$). However, it is doubtful that the DFT energies are sufficiently reliable to determine relative ordering.[25,26] A potential energy scan (redundant coordinate) extending the axial Ir−P distance in $\mathbf{1}^{T6}$ indicates a low barrier of ~1 kcal for complete triphos arm dissociation and a facile conversion to 5-coordinate triplet $\mathbf{1}^{T5}$. The transition state was located (Supporting Information) for the bromo system and is 1.0 kcal above the 6-coordinate triplet ($\mathbf{3}^{T6}$).

Mulliken atomic spin densities for the triplets are given in Table 3. In the 6-coordinate triplets, spin density is located primarily on the Ir center, two of the halogen atoms, and the elongated P atom (P3). Of the two halogen atoms with significant spin density, the halogen atom (X3) with the elongated bond dominates. This distribution and the geometry are consistent with a d^6 Jahn−Teller distorted triplet excited

Table 1. Experimental and Calculated Mean Metrical Parameters (Å and deg) for Ir(triphos)Cl_3

distance/angle[a]	experimental (1)	$\mathbf{1}^{S6}$
Ir−P	2.303(4)	2.391(15)
Ir−Cl	2.414(8)	2.475(10)
P−Ir−P	89.0(4)	89.0(17)
Cl−Ir−Cl	84.1(6)	86.6(13)
P−Ir−Cl	93.4(16)	92.2(32)
	176.0(4)	175.7(9)

[a]Mean values with standard deviations.

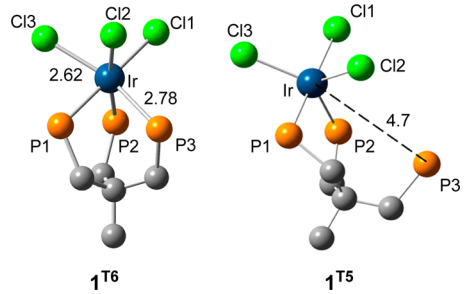

Figure 4. Optimized DFT (M06/LANL2DZ) 5- and 6-coordinate triplets $\mathbf{1}^{T5}$ and $\mathbf{1}^{T6}$ (hydrogen atoms and phenyl rings omitted).

dx.doi.org/10.1021/ic401835d | *Inorg. Chem.* 2013, 52, 12645−12654

Table 2. Metrical Parameters (Å and deg) for the 5- and 6-Coordinate Triplets

distance/angle[a]	1^{T6} (X = Cl)	1^{T5} (X = Cl)	3^{T6} (X = Br)	3^{T5} (X = Br)
Ir–P1	2.5006	2.3857	2.5054	2.4120
Ir–P2	2.3901	2.4258	2.4495	2.4460
Ir–P3	2.7768	4.7007[b]	2.8652	5.1938[b]
Ir–X1	2.4170	2.4360	2.5471	2.6344
Ir–X2	2.4941	2.4836	2.6369	2.5766
Ir–X3	2.6194	2.4388	2.8293	2.5827
P1–Ir–P2	88.09	88.64	88.15	89.29
P1–Ir–P3	78.60		83.17	
P2–Ir–P3	88.16		86.15	
X1–Ir–X2	86.76	93.00	85.52	90.58
X1–Ir–X3	97.00	94.00	97.74	90.85
X2–Ir–X3	86.26	113.96	84.03	113.28
P1–Ir–X1	178.08	179.00	177.87	177.62
P1–Ir–X2	94.91	86.00	93.06	87.54
P1–Ir–X3	82.18	86.40	84.68	88.56
P2–Ir–X1	90.38	91.77	93.06	92.80
P2–Ir–X2	171.69	113.37	172.62	113.20
P2–Ir–X3	101.84	131.88	103.34	133.32
P3–Ir–X1	102.52		95.15	
P3–Ir–X2	84.85		86.76	
P3–Ir–X3	158.01		164.33	

[a]Atom numbering from Figure 4. [b]Dangling P.

Table 3. Triplet Mulliken Atomic Spin Densities[a]

atom[a]	1^{T6}	1^{T5}	3^{T6}	3^{T5}
Ir	1.27	1.39	1.17	1.23
P1	0.01	−0.03[b]	0.01	−0.02[b]
P2	−0.01	0.10	−0.01	0.08
P3	0.17	0.00[c]	0.17[a]	0.00[c]
X1	0.15	0.06[b]	0.20	0.09[b]
X2	0.02	0.27	0.01	0.35
X3	0.34[a]	0.19	0.42[a]	0.25

[a]Atom numbering from Figure 4. [b]Axial ligand. [c]Dangling P.

state of primarily ligand field (LF) character with an unpaired electron in a t_{2g}-type orbital on the Ir center and an unpaired electron in an e_g-type M-L antibonding orbital (d_{z^2}). On moving to the more stable trigonal-bipyramidal 5-coordinate triplet, spin density on the Ir center increases slightly and shifts away from the dangling P atom (P3) and the axial P (P1) and halogen (X1) atoms.

Optimization of the triplet structure of $\mathbf{1}^{T5}$ as a singlet yielded square-pyramidal, 5-coordinate Ir(κ^2-triphos)Cl_3 ($\mathbf{1}^{S5}$, Figure 5) at 25.3 kcal above $\mathbf{1}^{S6}$ putting it 17.8 kcal lower in energy than triplet $\mathbf{1}^{T5}$. It is presumably 5-coordinate $\mathbf{1}^{S5}$ that is trapped by py or PPh_2Et or, in the absence of a trapping ligand, oligomerizes to produce **5**. It should be noted that trapping $\mathbf{1}^{S5}$ with py or PPh_2Et should give the *meridional* isomer, as is observed experimentally. Attempts to optimize (gas phase) the alternate isomer with a Cl atom in the axial position yielded a structure with the same Ir center geometry as in $\mathbf{1}^{S5}$ (axial P) but with the dangling P group in a slightly more stable (2 kcal) orientation. However, optimization of the axial-Cl isomer in CH_2Cl_2 (pcm model) did yield a stationary point structure ($\mathbf{1}^{S5'}$·**DCM**, Figure 5), evidently stabilized by the polar medium but less stable than the geometry of $\mathbf{1}^{S5}$.

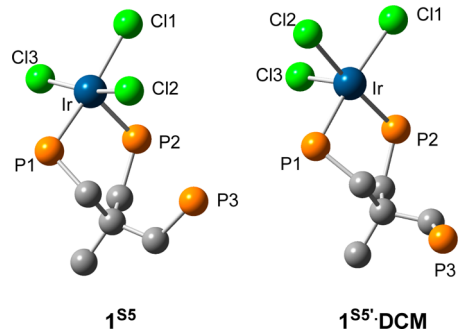

Figure 5. Optimized DFT (M06/LANL2DZ) 5-coordinate singlet structures for **1** (hydrogen atoms and phenyl rings omitted, gas phase for $\mathbf{1}^{S5}$, in dichloromethane for $\mathbf{1}^{S5'}$·**DCM**).

Time-dependent DFT (TDDFT) (CAM-B3LYP/LANL2DZ) calculations were used to obtain vertical transition energies and oscillator strengths for **1** and **3** and to simulate the absorption spectra (Supporting Information). A good match with the experimental spectra is obtained with a set of weak transitions at the UV–vis edge and stronger transitions deeper into the uv. The four lowest vertical singlet and triplet transitions for **1** are listed in Table 4. Each singlet transition has a matching triplet transition at slightly lower energy, implying facile intersystem crossing from the singlet to the triplet manifold.

The orbital make up of the transitions from the TDDFT calculations is quite complex. Simplification was obtained through a natural transition orbital (NTO) treatment.[27] Each of the transitions is described by two dominant NTO sets. Those for the first singlet (similar for the first triplet) are pictured in Figure 6. The "destination" orbitals (top) are e_g-type and show Ir-ligand σ-antibonding character. The departure orbitals are t_{2g}-type with contributions from the π-type p-orbitals of the Cl atoms. The NTO sets for the other three transitions (Supporting Information) are closely related, differing mostly in which Ir d- and Cl p-orbitals are involved. Thus, all of the transitions can be described as LF transitions.

DISCUSSION

In keeping with the known photochemistry of many Ir(III), Rh(III), and other low spin d^6 complexes,[28,29] the photolysis of **1** and **3** is dominated by ligand dissociation. Either halide ligand or triphos ligand arm dissociation is possible, but the photoproducts for **1** and **3** clearly indicate that triphos ligand arm dissociation dominates. (The alternative of halide dissociation/substitution followed by thermal halide displacement of the triphos ligand arm is very unlikely given the stability of Ir(triphos)X_3 to py.) This is not unexpected as halide photodissociation is disfavored in organic solvents because of poor charge solvation.[30]

Once formed, the photogenerated 5-coordinate intermediate would be susceptible to ligand coordination. In the absence of added ligand, several possibilities exist. Recoordination of the triphos arm would return the intermediate to **1** or **3**. If recoordination is slow, halide bridges with other Ir centers could form or the dangling triphos arm could coordinate to another Ir center forming a triphos bridge. Such bridged structures (Figure 7) are likely elements of photoproducts **5** and **6** and these compounds are formulated as oligomeric $[Ir(triphos)Cl_3]_n$ and $[Ir(triphos)Br_3]_n$. (Dimerization of *mer*-$Ir(Et_2S)_3Cl_3$ by photodissociation of Et_2S has been reported.[31])

dx.doi.org/10.1021/ic401835d | *Inorg. Chem.* 2013, 52, 12645–12654

Table 4. Lowest Four Singlet Vertical Transitions for 1^{S6} and Their Corresponding Triplet Transitions

singlets				triplets			
no.	λ, nm	osc. strength	contributions (≥5%)	no.	λ, nm	contributions (≥5%)	S-T gap (kcal/mol)
1	380	0.0015	H-3→LUMO (46%) H-2→L+1 (9%) H-3→L+3 (7%)	2	416	H-3→LUMO (36%) H-2→L+1 (8%) H-3→L+3 (7%) H-1→LUMO (9%)	−6.5
2	377	0.0139	H-2→LUMO (41%) H-2→L+3 (5%) H-3→L+1 (11%) H-5→LUMO (5%)	1	418	H-2→LUMO (40%) H-2→L+3 (10%) H-3→L+1 (6%) H-3→LUMO (6%)	−7.4
3	374	0.0115	H-4→L+1 (42%) HOMO→L+1 (22%)	3	410	H-4→L+1 (28%) HOMO→L+1 (28%) H-1→L+1 (6%) H-21→L+1 (5%)	−6.5
4	344	0.0006	HOMO→LUMO (32%) H-4→LUMO (24%) H-3→L+1 (11%)	4	391	HOMO→LUMO (26%) H-4→LUMO (19%) H-3→L+1 (6%) HOMO→L+3 (5%) H-4→L+1 (5%) H-21→LUMO (5%)	−9.9

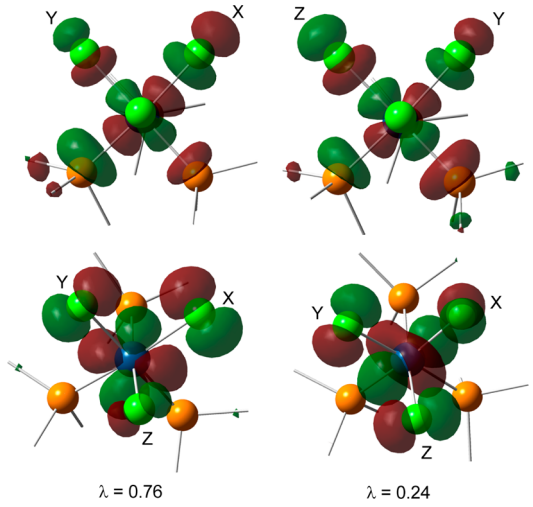

Figure 6. Natural transition orbital (NTO) sets for the first singlet excited state of 1^{S6} (isovalue = 0.04). The "destination" orbital is on the top and the "departure" orbital is on the bottom, and λ is the NTO eigenvalue for each set. The X, Y, and Z axes were arbitrarily chosen but are consistent for all drawings. (C and H atoms omitted.).

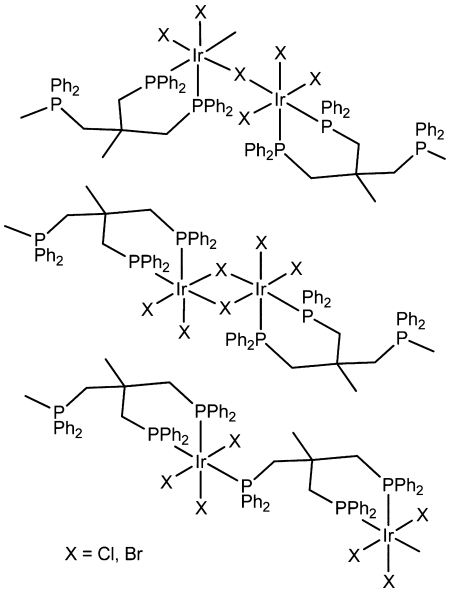

Figure 7. Proposed structural elements of **5** and **6**.

The solid-state NMR data, the far IR data, the formation of complex mixtures of products when **5** and **6** are first dissolved in pyridine, and the trapping of various amounts of solvent in the solid are all consistent with irregular bridged oligomeric structures. Interestingly, formation of **5** and **6** appears to be exclusively from oligomerization of the photogenerated 5-coordinate intermediate. If **1** or **3** were to react with the 5-coordinate intermediate through halide bridge formation dissolving **5** or **6** in pyridine would rupture the halide bridge and regenerate **1** or **3**. This is not observed. The implication is that the 5-coordinate intermediate is remarkably long-lived and recoordination of the dangling triphos arm relatively slow, allowing bimolecular reactions of the 5-coordinate intermediate to occur.

No doubt contributing to slow arm recoordination in the 5-coordinate intermediate is the square pyramidal geometry predicted by DFT. The open site of 1^{S5} is not adjacent to the dangling phosphine group and would require geometric isomerization to an alternative square-pyramidal structure ($1^{S5'}$·**DCM**) for recoordination of the dangling phosphine group. That the 5-coordinate intermediate has the structure of 1^{S5} is indicated by the initial formation of pyridine trapping product *mer*-Ir(κ^2-triphos)(py)Cl_3 (**7**) and PPh_2Et trapping product *mer*-Ir(κ^2-triphos)(PPh_2Et)Cl_3 (**10**) both of which can be envisioned as forming by pyridine or PPh_2Et coordination to the vacant site of 1^{S5}.

In agreement with previous conclusions on low-spin d^6 halide complex photochemistry,[28,29] the DFT and TDDFT calculations indicate that the phosphine group dissociation occurs through low-energy triplet excited states. These would be accessed through rapid internal conversion/intersystem crossing from initial excitation into the singlet manifold or possibly through direct excitation into the triplet manifold. This is consistent with the photochemistry wavelength independence

dx.doi.org/10.1021/ic401835d | *Inorg. Chem.* 2013, 52, 12645−12654

(313 and 380 nm and sunlight) of the complexes. The initially formed triplet LF Franck–Condon state would relax by Jahn–Teller distortion yielding 6-coordinate triplet structures $\mathbf{1}^{T6}$ or $\mathbf{3}^{T6}$. The 6-coordinate triplets then progress to 5-coordinate $\mathbf{1}^{T5}$ or $\mathbf{3}^{T5}$ through complete triphos ligand arm dissociation. (A similar 6-coordinate triplet was located by DFT for d^6 $[Ru(bpy)_2L_2]^{2+}$ and found to give ligand (L) dissociation.[32]) Subsequent intersystem crossing to singlet $\mathbf{1}^{S5}$ or $\mathbf{3}^{S5}$ would then open the complex to coordination of another ligand or reformation of **1** or **3**. This sequence, depicted in Scheme 3 for

Scheme 3

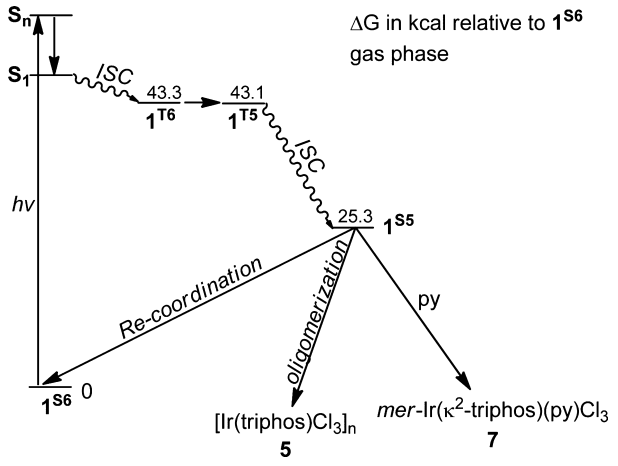

the chloro complexes, is analogous to that recently reported for $PtBr_6^{2-}$, a d^6 octahedral complex related to **1** and **3**.[33] Computational chemistry supported transient absorption spectroscopy of this Pt(IV) system indicates that initial excitation into the singlet manifold is followed by rapid intersystem crossing to the lowest-energy triplet with expulsion of a Br^- to give triplet 5-coordinate $PtBr_5^-$. The DFT calculated geometry for the relaxed 5-coordinate triplet is similar to that calculated here for $\mathbf{1}^{T5}$ and $\mathbf{3}^{T5}$ (distorted trigonal bipyramid). Intersystem crossing to square-pyramidal singlet $PtBr_5^-$ then opens the complex to ligand coordination (aquation or recombination with a Br^-) as predicted here for $\mathbf{1}^{S5}$ and $\mathbf{3}^{S5}$.

As mentioned in the introduction we began this study with the rather naive expectation of observing halogen photoelimination from **1** and **3**. This expectation was partly based on the halogen photoelimination from the related Pt(IV) d^6 complexes PtL_2X_3R (L = a phosphine; X = Cl, Br; R = Cl, Br, aromatic group).[1] At this juncture, we believe the difference between the Pt complexes and **1** and **3** is the character of the lowest-energy excited states. All of the above data point to a high degree of LF character in the lowest-energy excited states of **1** and **3**. In contrast, the Pt complex lowest-energy excited states have significant halogen lone-pair-to-Pt charge transfer (LMCT) character yielding radical density at the halogens in conjunction with a weakening of the Pt–X bonds.[1] We are still working out the likely pathways, but the result of radical halogen character in the excited state appears to be net elimination of X_2. Although less common than heterolytic ligand dissociation, photolytic radical reactivity has been observed for some d^6 complexes, especially on excitation into higher energy CT bands.[34−37]

In contrast to **1** and **3**, which photoeliminate a triphos arm, complexes **7** and **8** probably photoeliminate a chloride ligand along the Cl–Ir–Cl axis. This is suggested by Adamson's Rules, developed for d^3 complexes but also applicable to d^6 complexes, which state that ligand dissociation will occur along the weakest ligand field axis.[38−40] The isomerization of **7** and **8** to their *facial* isomers **9** and **11** likely occurs by a pathway similar to that in the photochemistry of **1** and **3**. This is illustrated for **8** in Scheme 4, where 5-coordinate triplet $\mathbf{8}^{T5}$ undergoes intersystem crossing to 5-coordinate singlet $\mathbf{8}^{S5}$. Recoordination of the chloride then yields **11**.

Finally, given the strong current interest in photoluminescent Ir(III) complexes, a comment on the different photoexcitation results for the above complexes should be made. A key difference is the nature of the lowest triplet excited state. The photoluminescent complexes generally contain ligands with extended π-systems.[3,4,41] This introduces low-lying intraligand triplet excited states that are inactive to ligand dissociation and phosphorescence dominates.

CONCLUSIONS

The photochemistry of d^6 Ir(triphos)Cl_3 (**1**) and Ir(triphos)Br_3 (**3**) is dominated by triphos ligand arm dissociation. Dissociation is proposed to occur through a triplet pathway, going first to a 6-coordinate Jahn–Teller distorted LF triplet excited state that transits by triphos arm dissociation to a 5-coordinate distorted trigonal bipyramidal triplet. Subsequent intersystem crosses then gives a long-lived, square pyramidal, 5-coordinate singlet that oligomerizes or is trapped by added ligands. No evidence was found for halogen elimination, as was observed for d^6 *trans*-$Pt(PEt_3)_2(R)X_3$ (R = Br, Cl, aromatic group; X = Cl, Br). The difference in the photochemistry of **1** and **3** and the Pt(IV) complexes is attributed to greater MLCT character in the lowest energy excited states.

Photoisomerization of *meridional* pyridine complexes (**7** and **8**) to the *facial* isomers (**9** and **11**) probably occurs by halide photodissociation where the 5-coodinate cationic intermediate is captured by the halide.

EXPERIMENTAL SECTION

General Procedures. Ir(triphos)Cl_3 (**1**)[15] and concentrated solutions of hydrogen peroxide in diethyl ether[42] were prepared by

Scheme 4

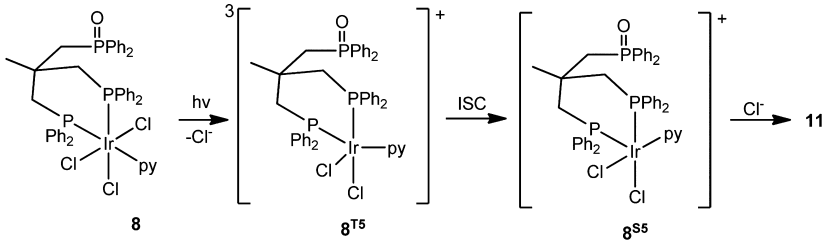

dx.doi.org/10.1021/ic401835d | Inorg. Chem. 2013, 52, 12645−12654

reported procedures. Reagents were purchased from commercial sources (Aldrich or Acros) and used as received. Experiments were performed under a dinitrogen or argon atmosphere in a Vacuum Atmospheres Corporation drybox or on a Schlenk line unless otherwise indicated. Solvents were dried, degassed, and stored under dinitrogen over 4 Å molecular sieves or sodium metal unless otherwise noted. Solution NMR spectra were recorded on Bruker AMX-250 or -300 spectrometer at ambient probe temperatures. Solid state ^{31}P NMR spectra were recorded on the Bruker AMX-300 spectrometer with MAS (magic angle spinning) at 5 kHz. NMR shifts are given in δ with positive values downfield of TMS (^{1}H and ^{13}C), external H_3PO_4 (^{31}P) and external ADP (ammonium dihydrogen phosphate) reference (solid state ^{31}P, δ 0). ^{13}C and ^{31}P NMR spectra were recorded in proton-decoupled mode. ALS Environmental performed the microanalyses. UV−vis spectra were recorded on a Cary 50 or Hewlett-Packard 8452 diode array spectrophotometer in 1 cm quartz cells. Photolyses were performed in 5 mm NMR tubes or 4 or 8 mL vials (borosilicate glass) using a Philips PL-S 9W/01, 9 W lamp (313 nm) or a Super Bright LEDs, RL5-UV0315-380 LED (380 nm) operated at 30 mA. The LED photon flux for the quantum yield determination was measured with a Newport 841-PE power meter equipped with an 818-UV detector.

Ir(triphos)Cl$_2$H (2). A 100 mL round-bottom flask was charged with a stirring bar and 38 mg (41 μmol) of **1** in 33 mL of 2-methoxyethanol. The mixture was refluxed under argon for 12 h. The volatiles were then removed in vacuo. The crude product was dissolved in 2 mL of dichloromethane and 75 mL of diethylether added to give a precipitate. The mixture was stored in a freezer for 30 min and then filtered through a fritted funnel (M) to isolate the precipitate, which was washed with 20 mL of diethylether and then extracted with acetonitrile. The volatiles were removed in vacuo from the extract giving 14.8 mg (41%) of solid pale yellow Ir(triphos)Cl$_2$H. ^{31}P NMR and ^{1}H NMR data match the literature values.[17]

^{31}P NMR (CD_2Cl_2, 101 MHz): −12.5 (d, J_{PP} = 11 Hz, 2P) −43.1 (t, J_{PP} = 11 Hz, 1P).

^{1}H NMR (CD_2Cl_2, 300 MHz): −7.91 (dt, J_{HP} = 188 Hz and J_{HP} = 10 Hz, 1H), 1.54 (s, 3H), 2.41 (m, 2H), 2.60 (m, 4H), 7.34 (m, 30H).

Ir(triphos)Br$_3$ (3). A 20 mL vial was equipped with a stirring bar and charged with 18.9 mg (20.5 μmol) of Ir(triphos)Cl$_3$ and 2.0 g (17 mmol) of KBr in 2−3 mL of freshly distilled acetone. The reaction mixture was stirred overnight at 40 °C. The completion of the reaction was confirmed by ^{31}P NMR spectroscopy. All volatiles were removed in vacuo, and the residue was extracted with dichloromethane (3 × 5 mL). The volatiles were removed from the extract in vacuo leaving a solid, which was washed with 2 × 1 mL of acetonitrile, 0.5 mL of water, and 2 mL of diethylether and dried in vacuo to give 18.7 mg (17.7 μmol, 86.3%) of solid pale yellow **3**.

^{31}P NMR (CH_2Cl_2, 101 MHz): −37 (s).

^{1}H NMR ($CDCl_3$, 300 MHz): 1.25 (s, 3H), 2.68 (d, J_{PH} = 7.06 Hz, 6H), 7.16 (m, 15H), 7.74 (br s, 15H).

Ir(triphos)Br$_2$H (4). A 50 mL round-bottom flask equipped with a stirring bar was charged with 32 mg (34.7 μmol) of **1**, 2 g of KBr, and 25 mL of bulk acetone. The mixture was stirred at 40 °C for 2 days. All volatiles were removed in vacuo, and the residue was extracted with dichloromethane. Removing the volatiles from the extract in vacuo yielded 28.3 mg (83.6%) of pale yellow Ir(triphos)Br$_2$H (**4**).

^{31}P NMR (CD_2Cl_2, 101 MHz): −13.1 (d, J_{PP} = 11 Hz, 2P) −50.8 (t, J_{PP} = 11 Hz, 1P).

^{1}H NMR (CD_2Cl_2, 300 MHz): −8.78 (dt, J_{HP} = 181, 9 Hz, 1H), 1.55 (s, 3H), 2.39 (m, 2H), 2.67 (m, 4H), 7.68−6.89 (m, 30H).

[Ir(triphos)Cl$_3$]$_n$ (5). A 4 mL vial was charged with 10 mg (10.9 μmol) of Ir(triphos)Cl$_3$ **1** and 1 mL of dichloromethane. The resulting yellow solution was photolyzed with a 313 nm light source. The yellow solution slowly bleached, and a yellowish precipitate formed. The photolysis was judged complete when an aliquot showed no ^{31}P NMR peaks. The volatiles were then removed in vacuo to yield the yellow solid product in quantitative yield. The product is insoluble in common organic solvents but dissolves readily in pyridine (see below). The results were identical when the experiment was repeated in air or with added 1-hexene (100 fold excess). Anal. Calc. (found) for $C_{41}H_{39}Cl_3IrP_3\cdot 0.3CH_2Cl_2$: C: 53.34 (52.29), H: 4.26 (4.21). The presence of the $0.3CH_2Cl_2$ was confirmed by ^{1}H NMR spectroscopy of the analytical sample dissolved in pyridine-d_5. A second sample was similarly analyzed and showed $0.45CH_2Cl_2$. See Supporting Information for solid-state ^{31}P NMR and IR spectra.

[Ir(triphos)Br$_3$]$_n$ (6). This was made in the same way as **5** with 11 mg (10.4 μmol) of Ir(triphos)Br$_3$ **3**. The yellow solid product was obtained in quantitative yield and is insoluble in common organic solvents. The results were identical when the experiment was repeated in air or with added 1-hexene (100 fold excess).

mer*-Ir(κ^2-triphos)(pyridine)Cl$_3$ (7).** A 50 mL sealable tube was charged with 64.4 mg (69.92 μmol) of **5**, and 25 mL of previously degassed pyridine was added. The tube was sealed, and the homogeneous mixture was heated at 120 °C overnight. (Caution!*** *This is above the boiling point of pyridine and the tube will be pressurized.*) The volatiles were then removed in vacuo yielding the yellow, air-sensitive, solid product in quantitative yield. Complex **7** was difficult to purify being always contaminated with small amounts of **8**.

^{31}P NMR ($CDCl_3$, 101 MHz): −26.5 (br s, 1P), −29.1 (dd, J_{PP} = 24 Hz, J_{PP} = 2 Hz, 1P), −41.0 (d, J_{PP} = 24 Hz, 1P).

^{31}P NMR (pyridine, 101 MHz): −26.3 (d, J_{PP} = 4 Hz, 1P), −27.9 (dd, J_{PP} = 24 Hz, J_{PP} = 4 Hz, 1P), −41.1 (d, J_{PP} = 24 Hz, 1P).

^{31}P NMR (C_6D_6, 101 MHz): −26.0 (d, J_{PP} = 4 Hz, 1P), −28.1 (dd, J_{PP} = 24 Hz, J_{PP} = 4 Hz, 1P), −41.5 (d, J_{PP} = 24 Hz, 1P).

^{31}P NMR (CD_3NO_2, 101 MHz): −26.2 (br d, J_{PP} = 3 Hz, 1P), −29.0 (dd, J_{PP} = 24 Hz, J_{PP} = 3 Hz, 1P), −40.9 (d, J_{PP} = 24 Hz, 1P).

^{1}H NMR ($CDCl_3$, 300 MHz): 8.97 (m, 2H), 8.07 (m, 2H), 7.71 (m, 7H), 7.26 (m, 22), 6.82 (m, 2H), 3.25 (m, 2H), 2.74 (m, 2H), 2.17 (br d, J = 2.4, 1H), 1.91 (br d, J = 2.4, 1H) and 1.23 (br s, 3H).

***mer*-Ir(κ^2-P,P-triphosO)(pyridine)Cl$_3$ (8).** Complex **7** was dissolved in 2−3 mL of dichloromethane, and a few drops of a concentrated solution of hydrogen peroxide in diethyl ether was added with stirring. The volatiles were removed in vacuo yielding yellow solid **8** in quantitative yield. Crystals for the X-ray analysis were grown by slow evaporation of a benzene solution of **8**. Anal. Calc. (found) for $C_{46}H_{44}Cl_3IrNOP_3$: C: 54.25 (53.63, 53.48), H: 4.36 (4.66, 4.66), N: 1.38 (1.41, 1.42).

^{31}P NMR (CDCl3, 101 MHz): 27.1 (s, 1P), −27.8 (d, J_{PP} = 24 Hz, 1P), −42 (d, J_{PP} = 23 Hz, 1P).

^{1}H NMR (CDCl3, 300 MHz): 8.95 (m, 2H), 8.2 (m, 2H), 8.1 (m, 2H), 7.9 (m, 2H), 7.7 (m, 1H), 7.6 (s, 1H), 7.30 (m, 19), 6.97 (m, 2H), 6.9 (t, 2H), 3.7 (m, 1H), 2.95 (m, 2H), 2.7 (m, 1H), 2.5 (m, 1H), 1.7 (m, 1H) and 1.55 (s, 3H).

Photolysis of *mer*-Ir(κ^2-P,P-triphosO)Cl$_3$ (8). Complex **8** (10 mg, 10 μmol) was dissolved in 0.5 mL of pyridine and photolyzed at 313 nm in 3 min intervals in a standard 5 mm NMR tube (N_2 atmosphere). The complex underwent photochemical isomerization to *fac*-Ir(κ^2-P,P-triphosO)(pyridine)Cl$_3$ (**11**) as shown by ^{31}P NMR spectroscopy. Similar experiments with **8** dissolved in dichloromethane, $CDCl_3$, and benzene gave no conversion after 30 min of irradiation.

Photolysis of Ir(triphos)Cl$_3$ (1) in pyridine. Complex **1** (6.0 mg, 6.5 μmol) was added to 0.5 mL of pyridine and photolyzed at 313 nm in a standard 5 mm NMR tube under an N_2 atmosphere. The progress of the photolysis was periodically monitored by ^{31}P NMR spectroscopy. The first two minutes of photolysis showed only formation of *mer*-Ir(κ^2- triphos)(pyridine)Cl$_3$ (**7**). After 7 min, both **7** and *fac*-Ir(κ^2-triphos)(pyridine)Cl$_3$ (**9**) were present along with remaining **1**. After 20 min, **1** was completely consumed and the **7**:**9** (*mer*:*fac*) ratio was 1:1.3. Continued photolysis completely converted the mixture to the *fac* isomer **9**. Air exposure of solutions of **9** gave *fac*-Ir(κ^2-P,P-triphosO)(pyridine)Cl$_3$ (**11**).

***fac*-Ir(κ^2-triphos)(pyridine)Cl$_3$ (9).** A 50 mL Schlenk flask was charged with 34.0 mg (36.9 μmol) of **1** in 8 mL of pyridine and a stir bar. The sample was photolyzed under N_2 at 313 nm for 4 h with stirring. The completion of the reaction was determined by ^{31}P NMR spectroscopy. The volatiles were then removed in vacuo (1 day). The resulting yellow solid was dissolved in dichloromethane. The solution was filtered through diatomaceous earth and reduced to ∼0.5 mL. Addition of 3−4 mL of hexane resulted in an immediate precipitate.

dx.doi.org/10.1021/ic401835d | *Inorg. Chem.* 2013, 52, 12645−12654

The mixture was allowed to stand at −20 °C for 3 h and then filtered through diatomaceous earth. The precipitate/diatomaceous earth mix was washed with 2−3 mL of hexane and then extracted with 3−4 mL of dichloromethane. The volatiles were removed in vacuo from the extract yielding 32.1 mg of yellow solid **9** (32.1 μmol, yield 87%). During isolation, **9** isomerized to small amounts of *mer*-Ir(κ^2-triphos)Cl_3(py) **7**.

^{31}P NMR ($CDCl_3$, 101 MHz): −27.8 (d, J_{PP} = 2 Hz, 1P), −38.7 (d, J_{PP} = 2 Hz, 2P).

^{31}P NMR (pyridine, 101 MHz): −27.8 (d, J_{PP} = 2 Hz, 1P), −38.7 (d, J_{PP} = 2 Hz, 2P).

^{31}P NMR (benzene, 101 MHz): −27.8 (d, J_{PP} = 2 Hz, 1P), −38.7 (d, J_{PP} = 2 Hz, 2P).

^{1}H NMR ($CDCl_3$, 300 MHz): 0.56 (s, 3H), 2.33 (br s, 2H), 2.39 (m, 2H), 3.73 (m, 2H), 7.20 (m, 30), 7.61 (t, J_{HH} = 7.5 Hz, 1H), 7.93 (m, 2H), 8.48 (br s, 2H).

Photolysis of Ir(triphos)Cl_3 with PPh_2Et. Observation of *mer*-Ir(κ^2-triphos)(PPh_2Et)Cl_3 (10). A standard 5 mm NMR tube was charged with 7.0 mg (7.6 μmol) of **1** and 1 M PPh_2Et in ∼0.5 mL of CH_2Cl_2. The sample was photolyzed at 380 nm for 33 min. The ^{31}P NMR spectrum confirmed full conversion. The product, *mer*-Ir(κ^2-P,triphos)Cl_3(PPh_2Et), was not isolated or further characterized.

^{31}P NMR (CH_2Cl_2, 101 MHz): −16.8 (dd, J_{PP} = 442 Hz, 16 Hz, 1P, PPh_2Et), −28.0 (s, 1P), −35.6 (dd, J_{PP} = 442 Hz, 19 Hz, 1P, P *trans* to PPh_2Et), −48.8 (overlapping dd, J_{PP} = 19 Hz, 16 Hz, 1P).

***fac*-Ir(κ^2-P,P-triphosO)(pyridine)Cl_3 (11).** (a) A 20 mL borosilicate vial was charged with 20 mg (22 μmol) of **5** dissolved in 5−6 mL of pyridine. The sample was photolyzed in sunlight through a window for 6 days. After completion of the reaction (^{31}P NMR spectroscopy), the volume was reduced to about 1.5 and 15 mL of hexane was added. The resulting milky solution and precipitate were stored in freezer overnight. The precipitate was then recovered by filtration, washed with hexane, and dried in vacuo to yield 15.2 mg (69%) of yellow solid **11**. (b) A 20 mL vial was charged with 44.6 mg (48.4 μmol) of **1** in 10 mL of pyridine. The sample was photolyzed at 313 nm for 24 h and judged complete by ^{31}P NMR spectroscopy. The volume of the solution was then reduced to 2 mL, and about 15 mL of diethyl ether was added to precipitate the product. The product was recovered by filtration through a pipet filled with diatomaceous earth and washed several times with diethyl ether. Extraction with dichloromethane and final removal of the volatiles in vacuo yielded 10.3 mg (21%) of yellow solid **11**.

^{31}P NMR (dichloromethane, 101 MHz): 25.7 (s, 1P), −39.3 (s, 2P).

^{1}H NMR (CD_2Cl_2, 250 MHz): 1.26 (s, 3H), 2.54 (d, J_{PH} = 11 Hz, 2H), 2.96 (m, 2H), 3.92 (m, 2H), 7.29 (m, 29H), 7.75 (m, 2H), 7.96 (m, 2H), 8.6 (m, 2H).

Quantum Yield. A quartz UV/vis cuvette was charged with a magnetic stir bar and 2.0 to 2.5 mL of a 1 M pyridine solution in dichloromethane with 4.0 mg (4.3 μmol) of Ir(triphos)Cl_3 (greater than 99% absorbance at 380 nm). The sample was photolyzed with the 380 nm LED at a distance of 1.2 cm from the cuvette (flux = 2.84 × 10^{15} photons/sec) with periodic ^{31}P NMR spectroscopic monitoring. Two measurements gave quantum yields of 0.23 and 0.29 (0.25 ± 0.04).

DFT Calculations. Gaussian 09[43] with the M06[44] (X = Cl) or B3LYP[45] (X = Br) functional was used for all calculations (gas phase), except for the TDDFT calculation, which employed the CAM-B3LYP[46] functional. The LANL2DZ[47,48] basis set was employed for all atoms. Initial structures were derived from crystal coordinates and were modified with Gaussview[49] without simplification. All geometries were optimized without symmetry constraints. Analytical frequency calculations gave no imaginary frequencies for the complexes except for Ir(triphos)Cl_3 (**1**), which had a small imaginary frequency of −21 cm^{-1} associated with a phenyl ring rotation and for the transition state for the interconversion of $\mathbf{3}^{T6}$ and $\mathbf{3}^{T5}$. The redundant coordinate potential energy scan for $\mathbf{1}^{T6}$ employed the "ModRedundant" keyword and increased the Ir−P distance in 0.1 Å increments with a maximum of 10 refinement cycles between increments. Free energies, enthalpies, and entropies were calculated at 298.15 K and 1 atm. The validity of using gas phase energies was tested by including a solvent correction (pcm model) for the gas phase energies of **1**, $\mathbf{1}^{T6}$, and $\mathbf{1}^{T5}$. This did not significantly alter their relative energies (3 kcal/mol or less) indicating that the gas phase relative energies are adequate. Coordinates and energies are given in the Supporting Information.

■ ASSOCIATED CONTENT

Ⓢ Supporting Information

CIF files, ^{1}H and ^{31}P NMR spectra, IR spectra, and DFT data (coordinates, energies, NTO figures). This material is available free of charge via the Internet at http://pubs.acs.org.

■ AUTHOR INFORMATION

Corresponding Author

*E-mail: sharpp@missouri.edu.

Author Contributions

The manuscript was written through contributions of all authors. All authors have given approval to the final version of the manuscript.

Notes

The authors declare no competing financial interest.

■ ACKNOWLEDGMENTS

Support was provided by the U.S. Department of Energy, Office of Basic Energy Sciences (DE-FG02-88ER13880). We thank Dr. Charles Barns for X-ray data collection and processing, Dr. Wei Wycoff for assistance with the NMR measurements, and Dr. Richard Martin for helpful discussions on the TDDFT calculations. The computations were performed on the HPC resources at the University of Missouri Bioinformatics Consortium (UMBC).

■ REFERENCES

(1) Karikachery, A. R.; Lee, H. B.; Masjedi, M.; Ross, A.; Moody, M. A.; Cai, X.; Chui, M.; Hoff, C.; Sharp, P. R. *Inorg. Chem.* **2013**, *52*, 4113.

(2) Nocera, D. G. *Inorg. Chem.* **2009**, *48*, 10001.

(3) Williams, J. A. G.; Wilkinson, A. J.; Whittle, V. L. *Dalton Trans.* **2008**, 2081.

(4) Lowry, M. S.; Bernhard, S. *Chem.—Eur. J.* **2006**, *12*, 7970.

(5) Zanella, A. W.; Talebinasab-Sarvari, M.; Ford, P. C. *Inorg. Chem.* **1976**, *15*, 1980.

(6) Talebinasab-Sarvari, M.; Zanella, A. W.; Ford, P. C. *Inorg. Chem.* **1980**, *19*, 1835.

(7) Brookes, P. R.; Masters, C.; Shaw, B. L. *J. Chem. Soc. A* **1971**, 3756.

(8) Talebinasab-Sarvari, M.; Ford, P. C. *Inorg. Chem.* **1980**, *19*, 2640.

(9) Deeming, J. A.; E. Vassos, A. *J. Chem. Soc., Dalton Trans.* **1997**, 3519.

(10) Geoffroy, G. L.; Hammond, G. S.; Gray, H. B. *J. Am. Chem. Soc.* **2002**, *97*, 3933.

(11) Stössel, P.; Heins, W.; Mayer, H. A.; Fawzi, R.; Steimann, M. *Organometallics* **1996**, *15*, 3393.

(12) Feldman, J. D.; Peters, J. C.; Tilley, T. D. *Organometallics* **2002**, *21*, 4050.

(13) Turculet, L.; Feldman, J. D.; Tilley, T. D. *Organometallics* **2004**, *23*, 2488.

(14) Gloaguen, Y.; Jacobs, W.; de Bruin, B.; Lutz, M.; van der Vlugt, J. I. *Inorg. Chem.* **2013**, *52*, 1682.

(15) Geerts, R. L.; Huffman, J. C.; Westerberg, D. E.; Folting, K.; Caulton, K. G. *New J. Chem.* **1988**, *12*, 455.

(16) Merola, J. S.; Franks, M. A.; Frazier, J. F. *Polyhedron* **2013**, *54*, 67.

(17) Janser, P.; Venanzi, L. M.; Bachechi, F. *J. Organomet. Chem.* **1985**, *296*, 229.

(18) Jenkins, J. M.; Shaw, B. L. *J. Chem. Soc.* **1965**, 6789.
(19) Clark, R. J. H.; Williams, C. S. *Inorg. Chem.* **1965**, *4*, 350.
(20) Shaw, B. L.; Smithies, A. C. *J. Chem. Soc. A* **1967**, 1047.
(21) Nakamoto, K. *Infrared and raman spectra of inorganic and coordination compounds*, 4th ed.; Wiley and Sons: New York, 1986.
(22) Doskocz, M.; Malinowska, B.; Młynarz, P.; Lejczak, B.; Kafarski, P. Ç. *Tetrahedron Lett.* **2010**, *51*, 3406.
(23) Siegl, W. O.; Lapporte, S. J.; Collman, J. P. *Inorg. Chem.* **1971**, *10*, 2158.
(24) Heinze, K.; Huttner, G.; Zsolnai, L. *Chem. Ber.* **1997**, *130*, 1393.
(25) Takatani, T.; Sears, J. S.; Sherrill, C. D. *J. Phys. Chem. A* **2009**, *113*, 9231.
(26) Takatani, T.; Sears, J. S.; Sherrill, C. D. *J. Phys. Chem. A* **2010**, *114*, 11714.
(27) Martin, R. L. *J. Chem. Phys.* **2003**, *118*, 4775.
(28) Ford, P. C. *Coord. Chem. Rev.* **1982**, *44*, 61.
(29) Ford, P. C.; Wink, D.; Dibenedetto, J. In *Progress in Inorganic Chemistry*; John Wiley & Sons, Inc.: New York, 1983; p 213.
(30) Bergkamp, M. A.; Watts, R. J.; Ford, P. C. *J. Am. Chem. Soc.* **1980**, *102*, 2627.
(31) Kauffman, G. B.; Tsai, J. H.-S.; Gubelmann, M. H.; Williams, A. F. *J. Chem. Soc., Dalton Trans.* **1980**, 1791.
(32) Salassa, L.; Garino, C.; Salassa, G.; Gobetto, R.; Nervi, C. *J. Am. Chem. Soc.* **2008**, *130*, 9590.
(33) Zheldakov, I. L.; N. Ryazantsev, M.; Tarnovsky, A. N. *J. Phys. Chem. Lett.* **2011**, *2*, 1540.
(34) Ford, P. C.; Hintze, R. E.; Petersen, J. D. In *Concepts of Inorganic Photochemistry*; Adamson, A. W., Fleischauer, P. D., Eds.; Wiley-Interscience: New York, 1975; p 203.
(35) Langford, C. H.; Malkhasian, A. Y. S. *J. Am. Chem. Soc.* **1987**, *109*, 2682.
(36) Glebov, E. M.; Grivin, V. P.; Plyusnin, V. F.; Venediktov, A. B.; Korenev, S. V. *J. Photochem. Photobiol., A* **2010**, *214*, 181.
(37) Glebov, E. M.; Kolomeets, A. V.; Pozdnyakov, I. P.; Plyusnin, V. F.; Grivin, V. P.; Tkachenko, N. V.; Lemmetyinen, H. *RSC Adv.* **2012**, *2*, 5768.
(38) Adamson, A. W. *J. Phys. Chem.* **1967**, *71*, 798.
(39) Adamson, A. W.; Waltz, W. L.; Zinato, E.; Watts, D. W.; Fleischauer, P. D.; Lindholm, R. D. *Chem. Rev.* **1968**, *68*, 541.
(40) Zink, J. I. *Coord. Chem. Rev.* **2001**, *211*, 69.
(41) Flamigni, L.; Barbieri, A.; Sabatini, C.; Ventura, B.; Barigelletti, F. In *Photochemistry and Photophysics of Coordination Compounds II*; Springer: Berlin, Germany, 2007; p 143.
(42) Saito, I.; Nagata, R.; Yuba, K.; Matsuura, T. *Tetrahedron Lett.* **1983**, *24*, 1737.
(43) Frisch, M. J.; Trucks, G. W.; Schlegel, H. B.; Scuseria, G. E.; Robb, M. A.; Cheeseman, J. R.; Scalmani, G.; Barone, V.; Mennucci, B.; Petersson, G. A.; Nakatsuji, H.; Caricato, M.; Li, X.; Hratchian, H. P.; Izmaylov, A. F.; Bloino, J.; Zheng, G.; Sonnenberg, J. L.; Hada, M.; Ehara, M.; Toyota, K.; Fukuda, R.; Hasegawa, J.; Ishida, M.; Nakajima, T.; Honda, Y.; Kitao, O.; Nakai, H.; Vreven, T.; Montgomery, Jr., J. A.; Peralta, J. E.; Ogliaro, F.; Bearpark, M.; Heyd, J. J.; Brothers, E.; Kudin, K. N.; Staroverov, V. N.; Kobayashi, R.; Normand, J.; Raghavachari, K.; Rendell, A.; Burant, J. C.; Iyengar, S. S.; Tomasi, J.; Cossi, M.; Rega, N.; Millam, J. M.; Klene, M.; Knox, J. E.; Cross, J. B.; Bakken, V.; Adamo, C.; Jaramillo, J.; Gomperts, R.; Stratmann, R. E.; Yazyev, O.; Austin, A. J.; Cammi, R.; Pomelli, C.; Ochterski, J. W.; Martin, R. L.; Morokuma, K.; Zakrzewski, V. G.; Voth, G. A.; Salvador, P.; Dannenberg, J. J.; Dapprich, S.; Daniels, A. D.; Farkas, Ö.; Foresman, J. B.; Ortiz, J. V.; Cioslowski, J.; Fox, D. J. *Gaussian 09*, Revision B.01 or C.01 ed.; Gaussian, Inc.: Pittsburgh,PA, 2009.
(44) Zhao, Y.; Truhlar, D. G. *Acc. Chem. Res.* **2008**, *41*, 157.
(45) Becke, A. D. *J. Chem. Phys.* **1993**, *98*, 5648.
(46) Yanai, T.; Tew, D.; Handy, N. *Chem. Phys. Lett.* **2004**, *393*, 51.
(47) Hay, P. J.; Wadt, W. R. *J. Chem. Phys.* **1985**, *82*, 299.
(48) Wadt, W. R.; Hay, P. J. *J. Chem. Phys.* **1985**, *82*, 284.
(49) O'Boyle, N. M.; Tenderholt, A. L.; Langner, K. M. *J. Comput. Chem.* **2008**, *29*, 839.